54-37

# REGARDLESS-OF-SPEED SUPERCONDUCTING LSM CONTROLLED-REPULSIVE MAGLEV VEHICLE

Kinjiro Yoshida, Tatsuya Egashira and Ryuichi Hirai
Department of Electrical Engineering
Faculty of Engineering, Kyusha University
10 - 1 6-chome Hakozaki Higashi - ku
Fukuoka, 812 JAPAN

## SUMMARY

This paper proposes a new repulsive Maglev vehicle which a superconducting LSM can levitate and propel simultaneously, independently of the vehicle speeds. The combined levitation and propulsion control is carried out by controlling mechanical-load angle and armature-current. Dynamic simulations show successful operations with good ride-quality by using a compact control method proposed here.

## INTRODUCTION

As a superconducting linear synchronous motor (LSM) repulsive Maglev vehicle, MLU002 in Japan is well-known all over the world [1]. This type of repulsive Maglev system is based on the electrodynamic repulsive forces which are generated on superconducting magnets moving over a series of short-circuited conducting coils. This Maglev system is simple but passive and also needs additional coils or sheets for levitation. The generated levitation forces are strongly dependent on the speed of moving magnets. In the speed range from a standstill to relatively high speeds, this Maglev system cannot levitate the vehicle. MLU002 takes off at the speed of about 150 Km/h.

This paper proposes a new repulsive Maglev vehicle system using a superconducting LSM which can propel and levitate simultaneously. This paper also presents a fundamental simulation study on a superconducting LSM Maglev vehicle which can produce repulsive force even at a standstill. With a concept proposed here, the vehicle can be levitated regardless of the vehicle speed. When the mechanical load-angle is controlled to be at a suitable position between half the pole-pitch and the pole-pitch, propulsion and levitation forces are produced simultaneously [2] in the superconducting LSM which has horizontally arranged armature windings on a guideway and horizontally-mounted superconducting magnets on the vehicle. The levitation force as well as the propulsion force are quite independent of the speed of superconducting magnets on the vehicle. By controlling the mechanical load-angle to be the pole-pitch and regulating the

125

armature-currents, the vehicle is levitated while it remains at a standstill [3]. After that, the vehicle starts running. The dynamic simulations show that the vehicle can run stably at the height of 15 cm, following a given speed pattern.
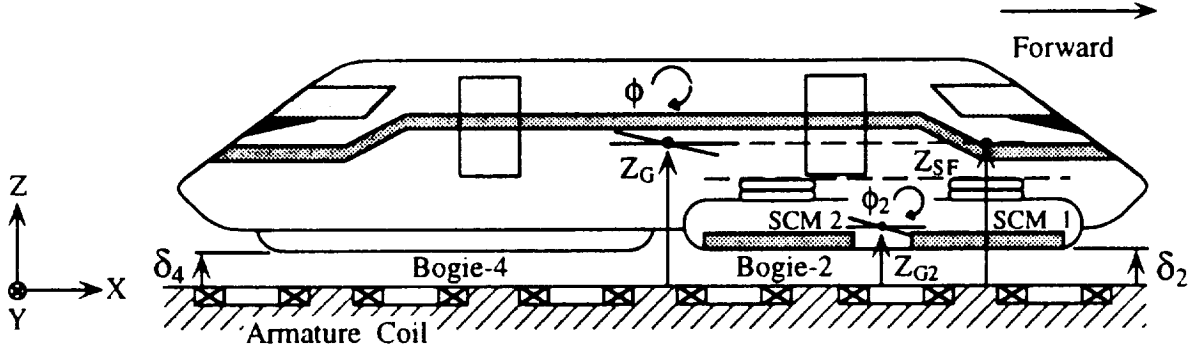


Figure.1  A Model for vehicle dynamics analysis

## EQUATIONS OF MOTION

Heave motions of the bogies and the cabin of the vehicle, which is illustrated in Fig. 1, are given as follows:

$$M_B \frac{d^2}{dt^2} Z_{G\,i} = \sum_{j=1}^{2} ( F_{Z,\,ij} - f_{s,\,ij} - f_{d,\,ij} ) - M_B\, g , \quad (i = 1, 2, 3, 4) \tag{1}$$

$$M_C \frac{d^2}{dt^2} Z_G = \sum_{i=1}^{4} \sum_{j=1}^{2} ( f_{s,\,ij} + f_{d,\,ij} ) - M_C\, g \tag{2}$$

$$f_{s,\,ij} = K_S\, \Delta l_{s,\,ij} \tag{3}$$

$$f_{d,\,ij} = K_D \frac{d}{dt} \Delta l_{s,\,ij} \tag{4}$$

where  $M_B$ = mass of bogie
  $M_C$ = mass of cabin
  $Z_{G\,i}$ = height of CG of bogie-i
  $Z_G$ = height of CG of cabin
  $F_{Z,\,ij}$ = levitation force
  $f_{s,\,ij}$ = restoring force of secondary suspension
  $f_{d,\,ij}$ = damping force of secondary suspension
  $\Delta l_{s,\,ij}$ = change of length in secondary suspension
  $K_S$ = stiffness of secondary suspension
  $K_D$ = damping constant of secondary suspension
  $g$ = acceleration of gravity

Propulsion motion of the vehicle is described by

$$M \frac{d}{dt} v_x = \sum_{i=1}^{4} \sum_{j=1}^{2} F_{X,ij} - K_A v_x^2 \tag{5}$$

where  $M = 4 M_B + M_C$ = mass of vehicle

$v_x$ = vehicle speed

$F_{X,ij}$ = thrust force acting on each superconducting magnet (SCM)

$K_A$ = coefficient of aerodynamic drag force

The pitching motions of bogies are

$$
I_{\phi B} \frac{d^2}{dt^2} \phi_i = - F_{X,i1} L_{BM} \sin(\phi_M + \phi_i) - F_{Z,i1} L_{BM} \cos(\phi_M + \phi_i)
$$
$$
- F_{X,i2} L_{BM} \sin(\phi_M - \phi_i) + F_{Z,i2} L_{BM} \cos(\phi_M - \phi_i)
$$
$$
+ (f_{s,i1} - f_{d,i1}) L_{BS} \cos(\phi_S - \phi_i) - (f_{s,i2} - f_{d,i2}) L_{BS} \cos(\phi_S + \phi_i) \tag{6}
$$
$$
(i = 1, 2, 3, 4)
$$

where  $L_{BM}$ = length between CG's of bogie and SCM

$L_{BS}$ = length between CG of bogie and joint of bogie to secondary suspension

$\phi_M$ = angle between $L_{BM}$ and X-axis

$\phi_S$ = angle between $L_{BS}$ and X-axis

$I_{\phi B}$ = moment of inertia of bogie for pitching motion

$\phi_i$ = pitching angle of bogie-i.

The pitching motion of the cabin is described by

$$
I_{\phi C} \frac{d^2}{dt^2} \phi = - \sum_{i=1}^{2} (f_{s,i1} - f_{d,i1}) L_f \cos(\phi + \phi_f)
$$
$$
+ \sum_{i=3}^{4} (f_{s,i2} - f_{d,i2}) L_f \cos(\phi + \phi_f)
$$
$$
- \sum_{i=1}^{2} (f_{s,i2} - f_{d,i2}) L_n \cos(\phi + \phi_n)
$$
$$
+ \sum_{i=3}^{4} (f_{s,i1} - f_{d,i1}) L_n \cos(\phi + \phi_n)
$$
$$
- \sum_{i=1}^{2} \frac{F_{X,i1} + F_{X,i2}}{2} \left\{ L_f \sin(\phi_f + \phi) + L_n \sin(\phi_n + \phi) \right\}
$$
$$
- \sum_{i=3}^{4} \frac{F_{X,i1} + F_{X,i2}}{2} \left\{ L_f \sin(\phi_f - \phi) + L_n \sin(\phi_n - \phi) \right\} \tag{7}
$$

where $L_f$, $L_n$ = length between CG of cabin and joint of cabin
to secondary suspensions measured far and near from CG of cabin

$\phi_f$, $\phi_n$ = angles between $L_f$ and X-axis and between $L_n$ and X-axis

$I_{\phi C}$ = moment of inertia of cabin for pitching motion

$\phi$ = pitching angle of cabin.

In this paper, the equations of motion are solved on the assumption that bogie-1 and 3 make the same motions as those of bogie-2 and 4, respectively.

## CONTROL METHOD

### Propulsion System

The demand patterns of effective value of armature-current $I_1$ and the mechanical load-angle $x_0$ are obtained as shown in equations (8) and (9), by applying the command acceleration-pattern $a_{x0}$ to the analytical equations for LSM Maglev system.

$$I_1^* = \frac{M}{4} \sqrt{ \left( \frac{a_{x0}}{K_X} \right)^2 + \left( \frac{g}{K_Z} \right)^2 } \tag{8}$$

$$x_0^* = \frac{\tau}{\pi} \tan^{-1} \left( - \frac{a_{x0} K_Z}{g K_X} \right) + \tau \tag{9}$$

where $K_X$, $K_Z$ = thrust and levitation-force coefficients

$I_1^*$ = demand pattern of effective value of armature-current

$x_0^*$ = demand pattern of mechanical load-angle

$\tau$ = pole-pitch.

In a repulsive-mode of the combined levitation and propulsion systems, $x_0^*$ should be controlled within the range $\frac{\tau}{2} \sim \frac{3}{2}\tau$ . In order to accomplish LSM operation at the demand mechanical load-angle $x_0^*$, the control law for $x_0$ based on PID regulator becomes equation (10).

$$\Delta x_0 = G_P ( v_x - v_{x0} ) + G_I \int ( v_x - v_{x0} ) \, dt + G_D ( \dot{v}_x - \dot{v}_{x0} ) \tag{10}$$

$$x_0 = x_0^* + \Delta x_0 \tag{11}$$

where $\Delta x_0$ = deviation of $x_0$

$G_P$, $G_I$, $G_D$ = feedback gains

$v_{x0}$ = command speed-pattern of vehicle.

In the levitation system with all the pitching motions neglected, equations of states, which are linearized about steady-state ($I_1^*$, $x_0^* = \tau$, $Z_{G0}$, $Z_{GB0}$) are expressed in the following matrix form:

$$\dot{X} = A X + B U \tag{12}$$

$$Y = C X = [\, \Delta Z_G \,] \tag{13}$$

with

$$X = [\; \Delta Z_G \quad \Delta Z_{GB} \quad \Delta \dot{Z}_G \quad \Delta \dot{Z}_{GB} \;]^T \tag{14}$$

$$U = [\, \Delta I_1 \,] \tag{15}$$

$$A = \begin{bmatrix} 0 & 0 & 1 & 0 \\[2mm] 0 & 0 & 0 & 1 \\[2mm] \dfrac{4\,K_S}{M_C} & \dfrac{2\,K_S}{M_C} & -\dfrac{8\,K_D}{M_C} & \dfrac{4\,K_D}{M_C} \\[3mm] \dfrac{K_S}{M_B} & \dfrac{K_{\delta Z} - K_S}{M_B} & \dfrac{2\,K_D}{M_B} & \dfrac{2\,K_D}{M_B} \end{bmatrix} \tag{16}$$

$$B = \begin{bmatrix} 0 & 0 & \dfrac{K_{IZ}}{M_B} & 0 \end{bmatrix}^T \tag{17}$$

$$C = [\, 1 \quad 0 \quad 0 \quad 0 \,] \tag{18}$$

where

$\Delta I_1$ = deviation of $I_1$

$\Delta Z_G$ = change in height of cabin from $Z_{G0}$

$Z_{G0}$ = steady-state height of cabin

$\Delta Z_{GB}$ = change in height of bogie from $Z_{GB0}$

$Z_{GB0}$ = steady-state height of bogie

$K_{\delta Z}$, $K_{IZ}$ = linearized coefficients of levitation-force with respect to airgap length and armature-current.

The control law of the levitation system is given by applying the theory of optimal servo control in the following form:

$$\Delta I_1(t) = -K_1 \Delta Z_G - K_2 \Delta Z_{GB} - K_3 \Delta \dot{Z}_G - K_4 \Delta \dot{Z}_{GB} - K_5 \int \Delta Z_G dt \qquad (19)$$

where $K_1, K_2, ..., K_5$ = feedback gains.

$K_1, K_2, ..., K_5$ are determined by solving the following performance index J based on LQ control theory.

$$J = \int_0^\infty \{ q_1 \Delta Z_G(t)^2 + q_2 \Delta Z_{G1}(t)^2 + q_3 \Delta \dot{Z}_G(t)^2$$

$$+ q_4 \dot{Z}_{G1}(t)^2 + r\Delta I_1(t)^2 \} dt \qquad (20)$$

where $q_1, q_2, q_3, q_4, r$ = weighting coefficients.

Therefore, the effective value of armature-current is calculated from

$$I_1 = I_1^* + \Delta I_1 \qquad (21)$$

The demand instantaneous value of the u-phase of armature-current can be obtained by

$$i_u^* = \sqrt{2} I_1 \cos \left( \frac{\pi}{\tau} \int_0^t v_{x0} dt + \frac{\pi}{\tau} x_0 + \frac{\pi}{2} \right) \qquad (22)$$

Note that $\frac{\pi}{2}$ in equation (22) is used for a starting position of the vehicle to coincide with the left-hand conductor of the u-phase coil.

## MAGLEV RUNNING SIMULATIONS

Basic behavior of the new Maglev vehicle which is levitated and propelled independently of vehicle speed according to a principle of the combined levitation and propulsion are analyzed numerically using equations (1) - (7) subject to the control method expressed by equations (10), (11), (19) and (21). The vehicle parameters are summarized in Table 1.

### Case Study for Acceleration and Deceleration of 1 m/s²

Figure 2 shows numerical experiments to show response to the command patterns which are given with dotted lines in Figs. 2 (a) - (d) for the speed and acceleration of the vehicle and airgap-lengths of the bogies. Just before 1 s and just after 69 s, the vehicle levitates steadily at standstill. The vehicle starts running in a levitated state with airgap lengths $\delta_2 = 15$ mm and $\delta_4 = 15$ mm.

130

## Table 1. Superconducting LSM Vehicle

| | | |
|---|---|---|
| **Superconducting Magnet :** | | |
| No. of Poles per one Bogie | P $=$ | 2 |
| Coil Length | $L_{SC}$ $=$ | 2.2 m |
| Coil Width | $W_{SC}$ $=$ | 0.5 m |
| Pole-Pitch | $\tau$ $=$ | 2.7 m |
| MMF | $I_{SC}$ $=$ | 700 kAT |
| **Armature Winding :** | | |
| Coil Length | $L_{AC}$ $=$ | 1.5 m |
| Coil Width | $W_{AC}$ $=$ | 0.6 m |
| Number of Turn | $T_a$ $=$ | 30 turns |
| **Mass :** | | |
| Mass of one Bogie | $M_B$ $=$ | 2 t |
| Mass of Cabin | $M_C$ $=$ | 10 t |
| **Secondary Suspension :** | | |
| Stiffness | $K_S$ | $= 1.3 \times 10^6$ N/m |
| Damping Constant | $K_D$ | $= 2.3 \times 10^5$ N $\cdot$ s/m |
| Natural Length | $l_0$ $=$ | 0.3 m |
| **Vehicle Size :** | | |
| Cabin Length | $L_C$ $=$ | 10.8 m |
| Cabin Width | $W_C$ $=$ | 1.5 m |
| Cabin Height | $H_C$ $=$ | 2.0 m |
| Bogie Height | $H_B$ $=$ | 0.5 m |
| **The Moment :** | | |
| the Moment of Inertia of Bogie for Pitching Motion | $I_{\phi B}$ $=$ | 4208 kg $\cdot$ m$^2$ |
| the Moment of Inertia of Cabin for Pitching Motion | $I_{\phi C}$ | $= 100533$ kg $\cdot$ m$^2$ |
| **Coefficient of aerodynamic force :** | $K_A$ | $= 1.305$ N $\cdot$ s$^2$/m$^2$ |

Figures 2 (a) and (b) show that the vehicle follows very well the command speed- and acceleration-patterns. Figures 2 (c) and (d) also show that the rear SCM2 of the bogie-2 and the front SCM1 of the bogie-4 follow very well the command airgap-length patterns, but the front SCM1 of the bogie-2 and the rear SCM2 of the bogie-4 do not follow that command patterns. During the acceleration phase, the SCM1's of the bogie-2 and 4 are higher and lower than the command value by about 1.5 cm, respectively, and during the deceleration phase vice versa. This is the reason why thrust and braking forces as shown in Fig. 2 (g) produce the pitching motions in the inverse direction of each other during acceleration and deceleration phases, respectively. Those pitching motions influence strongly only the front and rear SCM's in the vehicle. But, though the distance between the neighboring bogies is quite short, the secondary suspensions reduce the pitching motions of the cabin to about 67% as shown in Fig. 2 (I). Figures 2 (j), (k) and (m) show that the center of gravity (CG) of the vehicle does not change due to lack of heave motions in the SCM2 of the bogie-2 and the SCM1 of the bogie-4, which the heave motions of the CG's of bogie-2 and 4 cause as shown in Fig. 2 (n). It is thus found that the ride-quality is
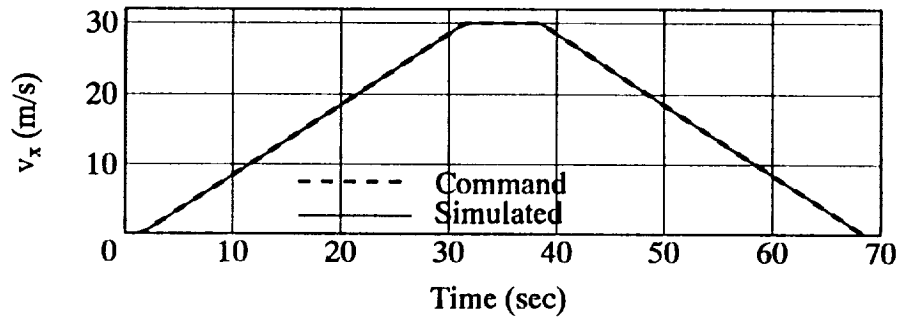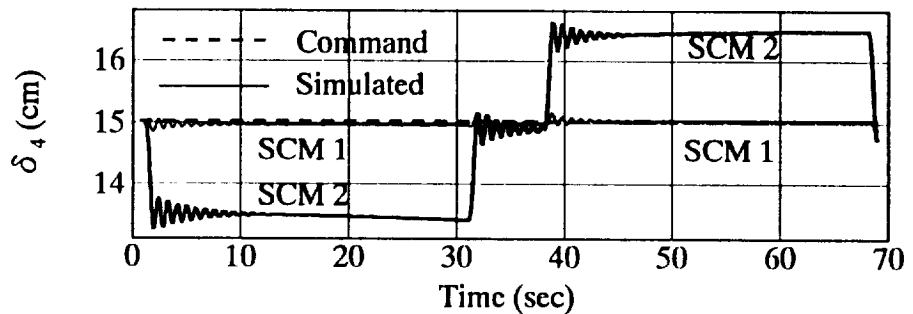
(a) Command and simulated vehicle speeds
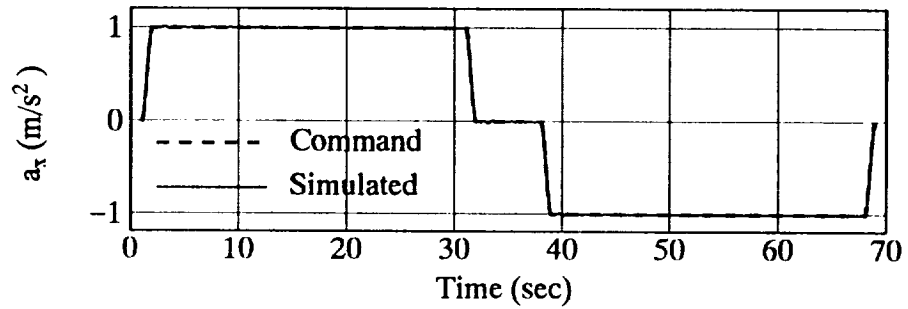
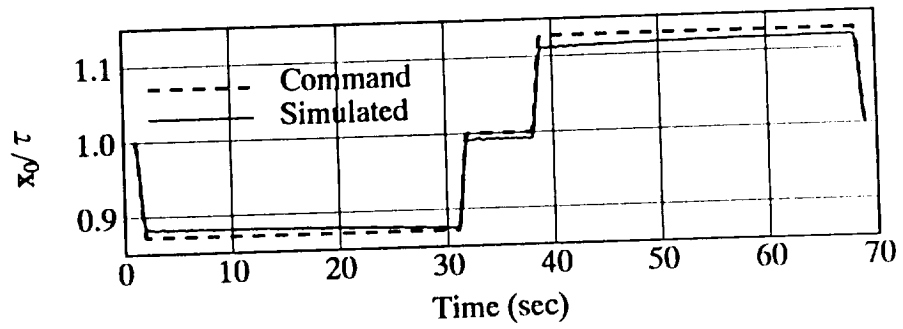(b) Command and simulated vehicle accelerations
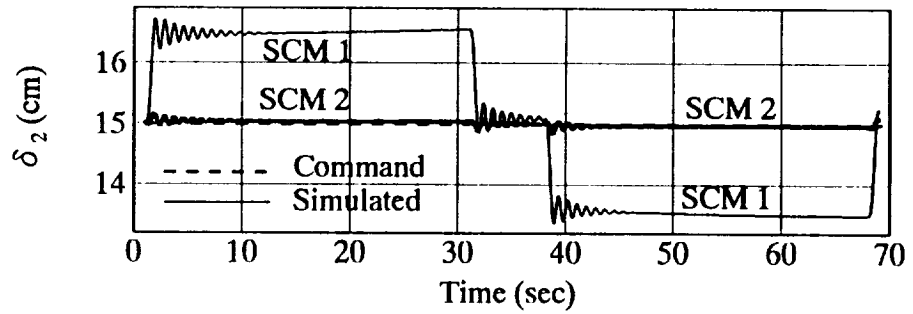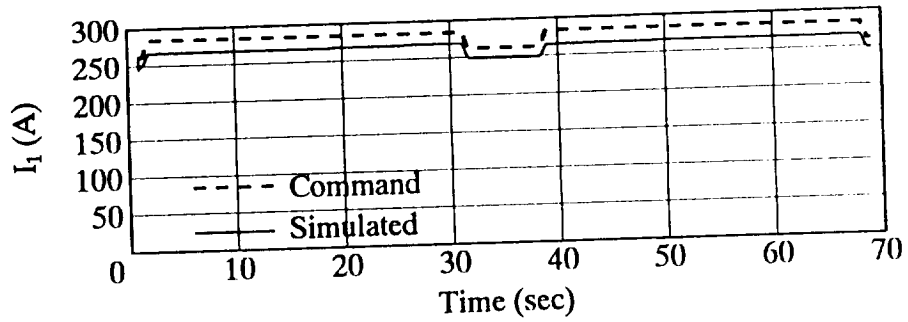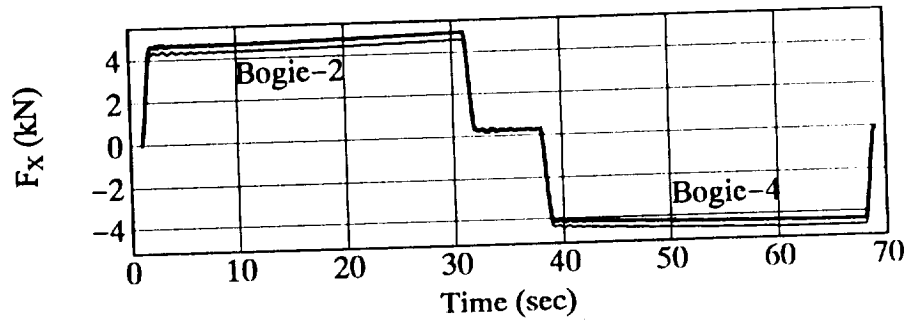
(c) Airgap length of bogie-2

(d) Airgap length of bogie-4

Figure. 2 Levitation and propulsion control for acceleration and deceleration of 1 m/s$^2$
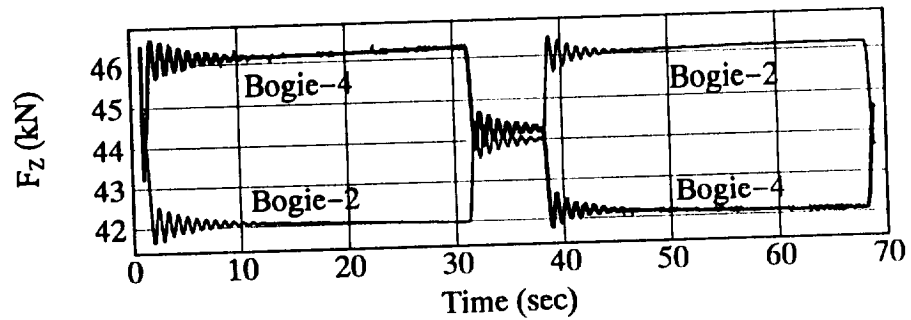
132

(e) Command and simulated mechanical load–angles
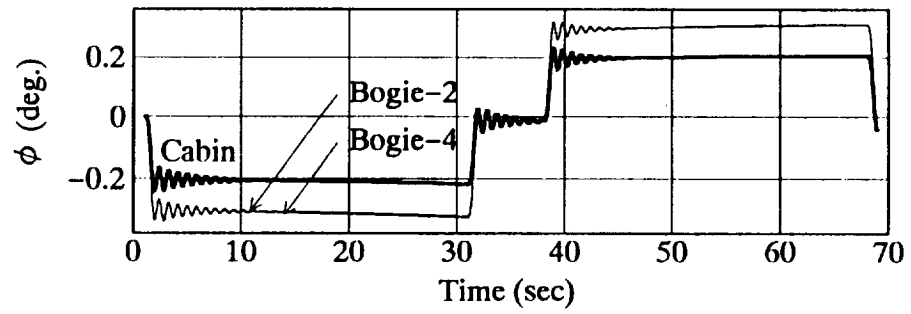


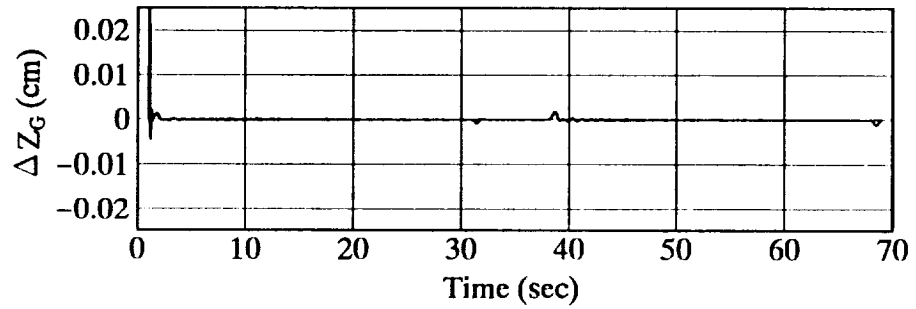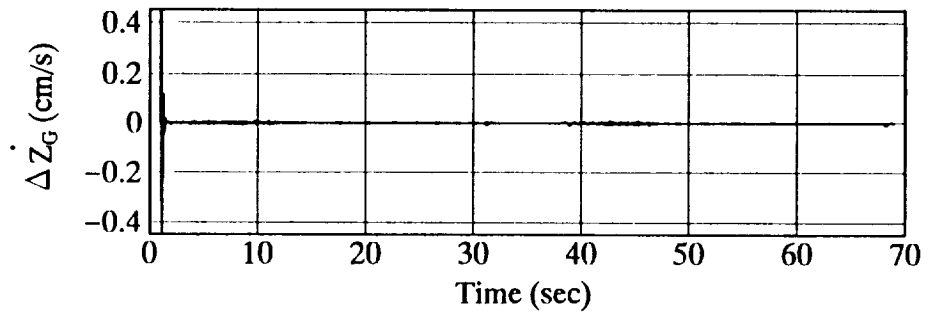(f) Command and simulated stator–currents



(g) Thrust force



(h) Lift force

Figure. 2 Levitation and propulsion control for acceleration and deceleration of 1 m/s$^2$

(i) Pitching angles of cabin and bogie-2 and 4



(j) Heave variation of cabin



(k) Heave velocity of cabin
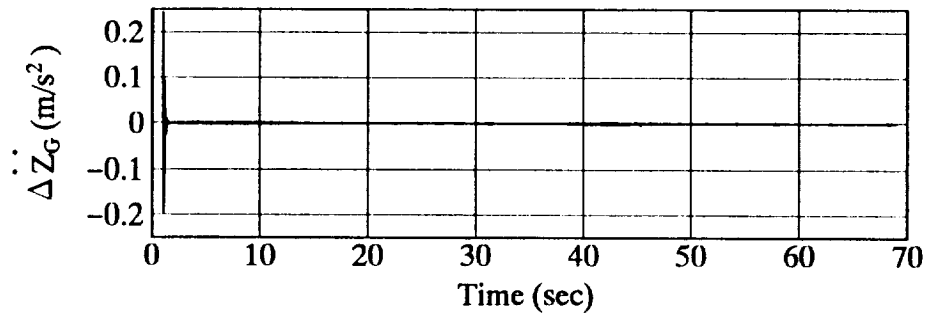


(l) Heave acceleration of cabin

Figure. 2 Levitation and propulsion control for acceleration and deceleration of 1 m/s²
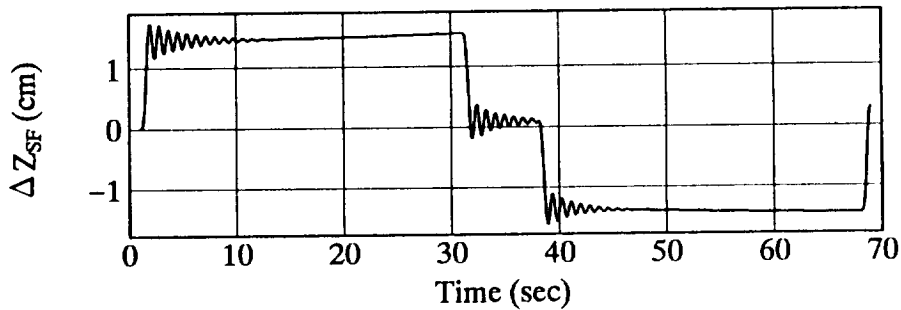
(m) Heave variation of front cabin above the secondary suspension
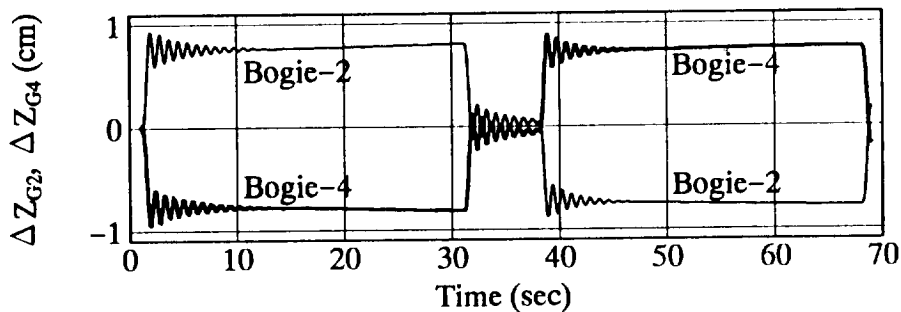


(n) Heave variations of CG of bogie-2 and 4

Figure. 2 Levitation and propulsion control for acceleration and deceleration of 1 m/s$^2$

very good around the CG of the cabin. Figure 2 (m) shows the heave variation of the front portion of the cabin above the secondary suspension measured far from the CG of the cabin which is about the same variation as +/- 1.5-cm-variation of SCM1 of the bogie-2 as shown in Fig. 2 (c). This variation is not so important, and its acceleration is much smaller than 0.1g. Therefore, the ride-quality near the front and rear portions of the vehicle is also very good.

Concerning the control of mechanical load-angle and armature-current, it is known from Figs. 2 (e) and (f) that, though a compact control method proposed here is used, the simulated results show a good agreement with the command patterns within a small error of about 6%. Figure 2 (f) also shows that the simulated current is smaller than the command one. This is due to the fact that the SCM2 of the bogie-4 heaved upward by 1.5 cm producing larger levitation-force than the SCM1 of the bogie-2 heaved downward by 1.5 cm.

Figure 3 shows numerical experiments for the case where the levitated vehicle is propelled with 3 times larger acceleration than that in Fig. 2. As shown in Figs. 3 (c) and (d), during the acceleration phase, airgap-length variations of the SCM1 of the bogie-2 and the SCM2 of the bogie-4 are proportionally 3 times larger and smaller than those of Fig. 3. It is known from Fig. 3 (f) that the armature-current is also controlled with about 3 times larger error than that in Fig. 2. But Figs. 3 (a) and (b) show for the vehicle to follow very well the command patterns. Figures 3 (j), (k) and (l) show the good ride-quality which is almost similar with that in Fig. 2. It is confirmed that a compact control method enables the vehicle to run stably even in this case.

## CONCLUSIONS

A new type of superconducting LSM Maglev vehicle system is proposed which can levitate and propel independently of the vehicle speeds. A compact control method is developed which is based on the concept of controlling the levitation system with armature-current and the propulsion system with mechanical load-angle. It is verified from dynamic simulations that the vehicle is controlled to follow very well the command speed pattern in both cases for accelerations of 1 m/s² and 3 m/s². Though the compact control method is applied, the vehicle is operated with very high ride-quality.

Operation in the range of $\frac{\tau}{2} \sim \frac{3}{2}\tau$ have never previously been used, but have recently been successfully demonstrated experimentally by us [4]. The present study gives a base for a large-scale new Maglev vehicle.

## ACKNOWLEDGMENTS

## REFERENCES

1. Fujie: Running Characteristics of the MLU002 Maglev Vehicle and Future Development Plan, Proc. Inter. Conf. Maglev '88 in Hamburg, June 1988, pp. 281-287.

2. K. Yoshida: Magnetic Levitation and Linear Motor, Science of Machine, Vol. 42, No. 4, 1990, pp. 468-474.

3. K. Yoshida and S. Nagao: Levitation and Propulsion Control Simulation of Regardless-of-Speed Superconducting LSM Repulsive Maglev Vehicle, Proc. of the 3rd Symposium on Electromagnetic Forces, June 1991, pp. 201-206.

4. K. Yoshida; H. Takami; N. Shigemi; and A. Sonoda: Repulsive-Mode Levitation and Propulsion Control of a Land Traveling Marine-Express Model Train ME03, Proc. of LDIA '95 Nagasaki, 1995, pp. 41-44.
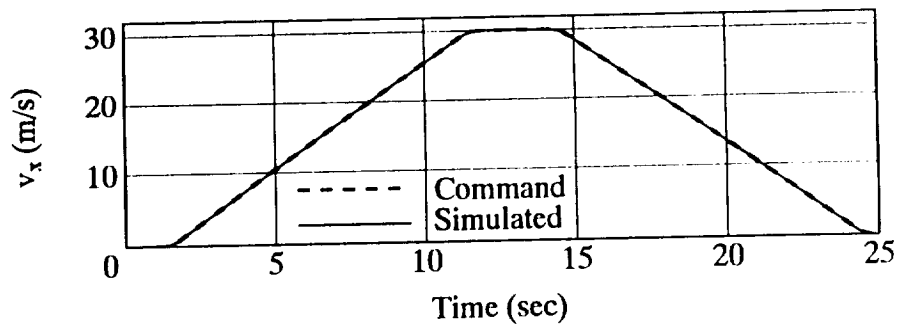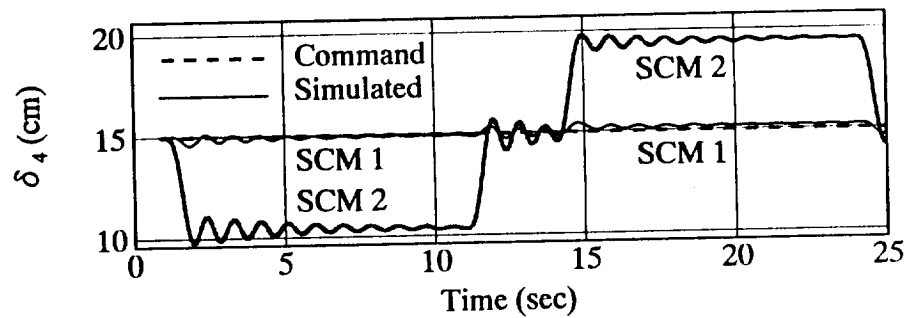
(a) Command and simulated vehicle speeds
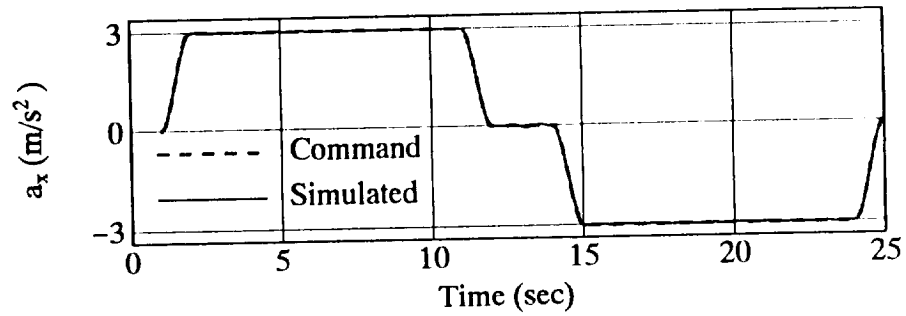
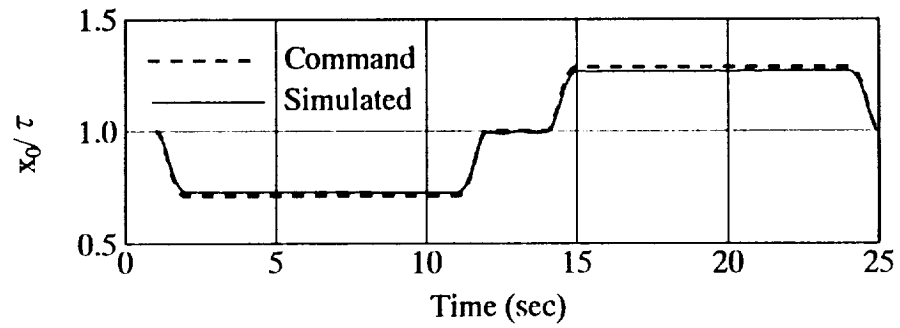(b) Command and simulated vehicle accelerations
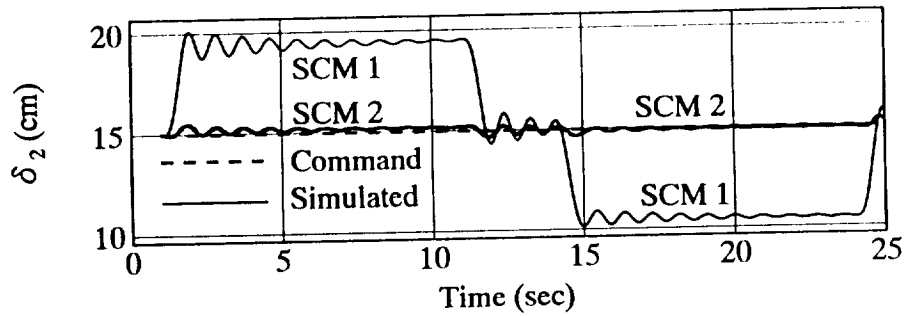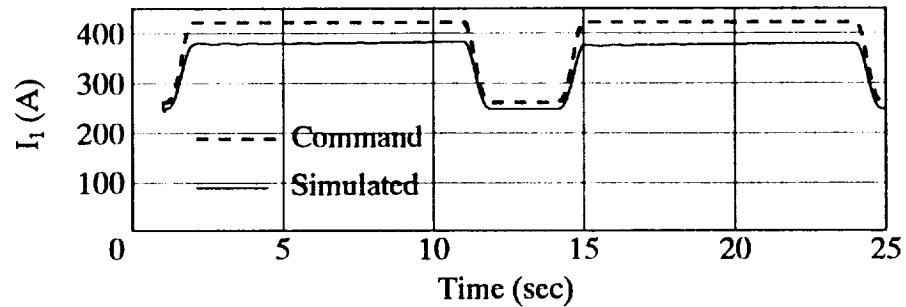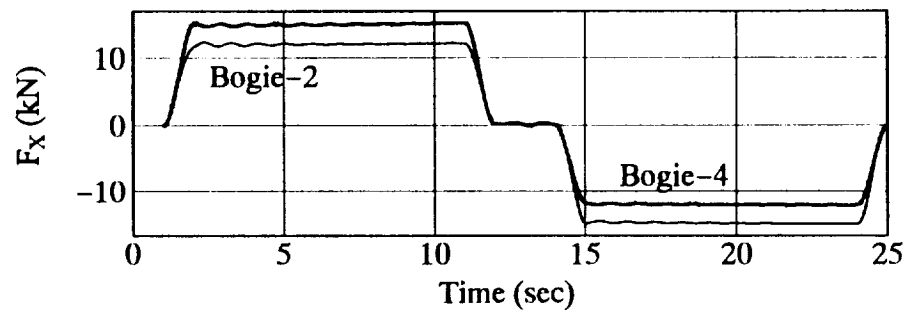
(c) Airgap length of bogie-2

(d) Airgap length of bogie-4

Figure. 3 Levitation and propulsion control for acceleration and deceleration of 3 m/s$^2$
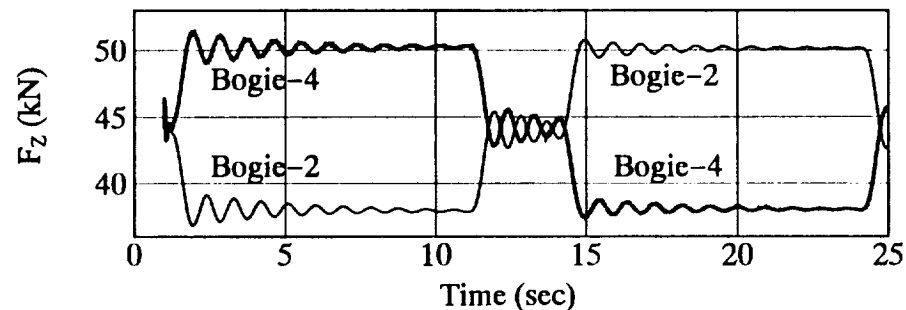
(e) Command and simulated mechanical load-angles
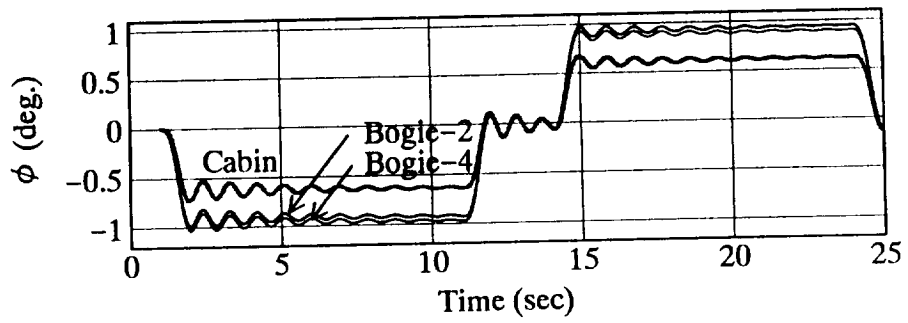


(f) Command and simulated stator-currents
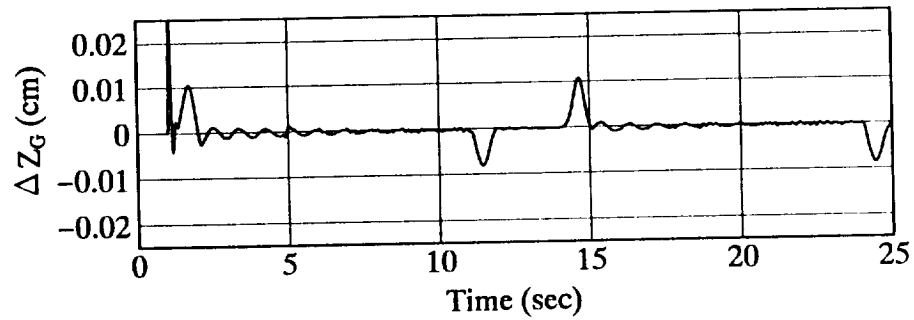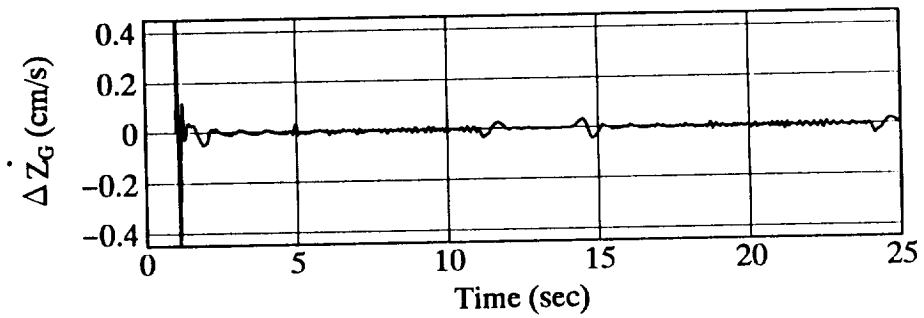


(g) Thrust force



(h) Lift force

Figure. 3 Levitation and propulsion control for acceleration and deceleration of 3 m/s²
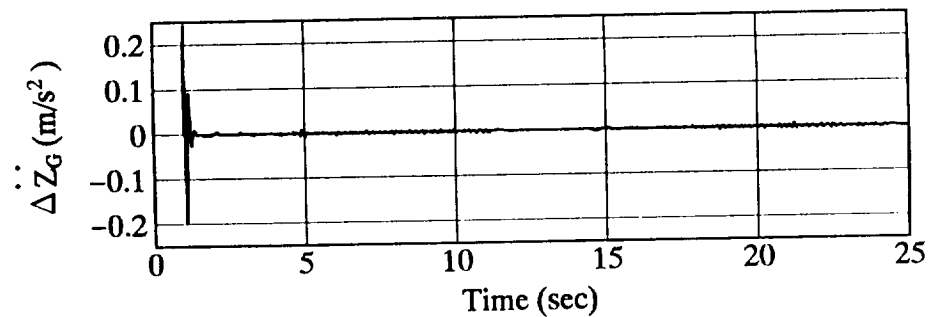
138

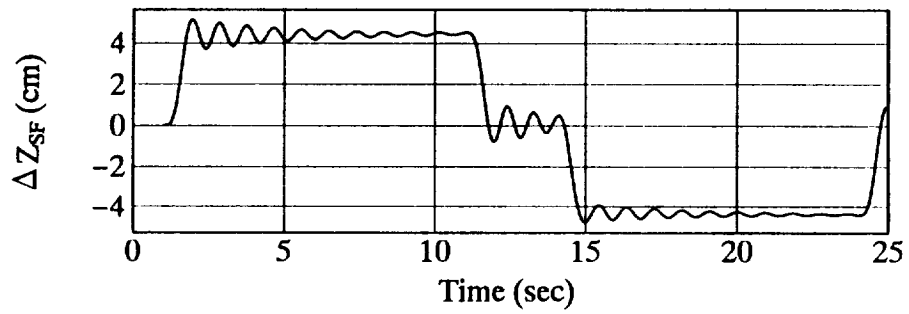(i) Pitching angles of cabin and bogie-2 and 4



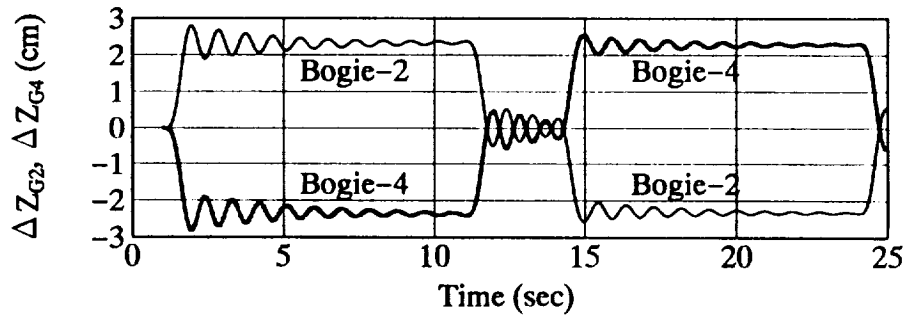(j) Heave variation of cabin



(k) Heave velocity of cabin



(l) Heave acceleration of cabin

Figure. 3 Levitation and propulsion control for acceleration and deceleration of 3 m/s²

139

(m) Heave variation of front cabin above the secondary suspension



(n) Heave variations of CG of bogie-2 and 4

Figure. 3 Levitation and propulsion control for
acceleration and deceleration of 3 m/s$^2$